Task-related oxygenation and cerebral blood volume changes estimated from NIRS signals in motor and cognitive tasks

Hirokazu Tanaka, Takusige Katura, Hiroki Sato

PII: S1053-8119(14)00167-0
DOI: doi: 10.1016/j.neuroimage.2014.02.036
Reference: YNIMG 11196

To appear in: *NeuroImage*

Accepted date: 19 February 2014

Please cite this article as: Tanaka, Hirokazu, Katura, Takusige, Sato, Hiroki, Task-related oxygenation and cerebral blood volume changes estimated from NIRS signals in motor and cognitive tasks, *NeuroImage* (2014), doi: 10.1016/j.neuroimage.2014.02.036

Task-related oxygenation and cerebral blood volume changes estimated from NIRS signals in motor and cognitive tasks

Hirokazu Tanaka[a*,†], *Takusige Katura*[b,†] *and Hiroki Sato*[b]

a. School of Information Science
Japan Advanced Institute of Science and Technology
1-1 Asahidai, Nomi, Ishikawa 923-1211, Japan

b. Central Research Laboratory, Hitachi, Ltd.
2520 Akanuma, Hatoyama, Saitama 350-0395, Japan

* Corresponding author
† Equally contributed

Text page: 32
Figures: 8
Abstract: 226 words
Introduction: 870 words
References: 54

Abbreviated Title: Task-Related Component Analysis±

Corresponding author:
Hirokazu Tanaka
Email: hirokazu@jaist.ac.jp
Tel: +81-761-51-1226
Fax: +81-761-51-1149

ABSTRACT

Although functional near-infrared spectroscopy (fNIRS) has an advantage of simultaneously measuring changes in oxy- and deoxy-hemoglobin concentrations (Δ[HbO] and Δ[HbR]), only few analysis approaches exploit this advantage. As an extension of our recently proposed method (task-related component analysis, TRCA), this study proposes a new analysis method that extracts task-related oxygenation and cerebral blood volume (CBV) changes. In the original formulation of TRCA, task-relatedness of a signal is defined as consistent appearance of a same waveform in every task block, thereby constructing task-related components by maximizing inter-block covariance. The new method proposes that, in addition to maximizing inter-block covariance, the covariance between task-related Δ[HbO] and Δ[HbR] is maximized ($TRCA^{+}$) or minimized ($TRCA^{-}$) so that oxygenation and CBV changes are maximally contrasted. The proposed method (collectively called $TRCA^{\pm}$) was formulated as a matrix eigenvalue problem, which can be solved efficiently with standard numerical methods, and was tested with a synthetic data generated by a balloon model, successfully recovering oxygenation and CBV components. fNIRS data from sensorimotor areas in a finger-tapping task and from prefrontal lobe in a working-memory (WM) task were then analyzed. For both tasks, the time courses and the spatial maps for oxygenation and CBV changes were found to differ consistently, providing certain constraints the parameters of balloon models. In summary. TRCA can estimate task-related oxygenation and CBV changes simultaneously, thereby extending the applicability of fNIRS.

Key words: Covariance Maximization; Inter-hemoglobin covariance; Balloon Model; Functional Neuroimaging; Optical Topography; Biomedical Data Analysis

1. INTRODUCTION

Among human neuroimaging modalities, functional near-infrared spectroscopy (fNIRS) has a unique advantage of simultaneously measuring oxy-hemoglobin (Δ[HbO]) and deoxy-hemoglobin (Δ[HbR]) concentration changes with multiple wavelengths of incident light. Extant studies have established that Δ[HbO] and Δ[HbR] are negatively correlated during neural activations (Devor et al., 2003; Malonek and Grinvald, 1996; Mayhew et al., 1999; Sheth et al., 2004; Tang et al., 2009) and positively correlated if they result from systemic factors or body movements (Cui et al., 2010; Yamada et al., 2012). Therefore, this hemoglobin covariation can be potentially informative to determine the origin of fNIRS signals. Nonetheless, most studies analyze Δ[HbO] and Δ[HbR] separately, or only Δ[HbO] due to its stronger signal-to-noise ratio. Only few studies exploited the hemoglobin covariation (Cui et al., 2010; Wylie et al., 2009; Yamada et al., 2012); for example, (Cui et al., 2010) proposed to use a running correlation between Δ[HbO] and Δ[HbR] to identify and remove movement related artifacts.

A recent series of studies from Das and colleagues demonstrated that, with a dual-wavelength optical imaging technique, intrinsic optical signals measured from the visual cortex of alert monkey consist of multiple, distinct time courses that reflect a stimulus-related and task-related component, respectively (Cardoso et al., 2012; Sirotin et al., 2012; Sirotin and Das, 2009; Sirotin et al., 2009). Their experiments employed green light (530 nm, an isobetic) that is absorbed in oxy- and deoxy-hemoglobin almost equally (thereby measuring total hemoglobin or cerebral blood volume (CBV)) and red light (605 nm) that is absorbed five-fold more strongly in deoxy- than oxy-hemoglobin (thereby measuring oxygenation). The oxygenation component was well predicted by simultaneously recorded local field potentials (LFPs) evoked by visual stimuli; hence this component was interpreted as stimulus related. The CBV component, in contrast, was not predicted by LFPs but rather entrained with the task's predictability such as rest durations and stimulus

presentation timings. Although intrinsic optical measurement of monkeys and fNIRS of humans differ in that reflected or scattered light is measured directly from the exposed cortical surface or indirectly through skin and skull, they both rely on the fact that oxy- and deoxy-hemoglobin have distinct absorption coefficients according to the wavelength of incident light. It is thus conceivable that fNIRS signals contain multiple components with distinct physiological origins.

Understanding systemic and neuronal origins of fNIRS signals is not only of neurobiological interest for the mechanisms of neurovascular coupling but also of practical interest of avoiding false positives in analyzing fNIRS data. A number of recent studies demonstrated that fNIRS signals contain hemoglobin changes that originate not only from neuronal activation but also from systemic variations such as heart rate and blood pressure (Katura et al., 2006) and from skin blood flow (Kirilina et al., 2012; Takahashi et al., 2011; Tong et al., 2011), leading to inflated statistics and potential false positives (Tachtsidis et al., 2009). Methods for separating multiple components of distinct origins are of critical importance. A number of previous studies have tackled this challenge by developing novel signal processing methods. Approaches based on independent component analysis, for example, identified and separated putative cerebral hemodynamic and systemic responses by assuming different spatial distributions (Katura et al., 2008; Kohno et al., 2007). Although the assumption of distinct spatial distribution sounds reasonable, it is justified only for experimental tasks whose activation maps are well understood. Traditionally, the total hemoglobin concentration change (i.e., the sum of Δ[HbO] and Δ[HbR]) has been used as an estimate of total blood volume (Wyatt et al., 1990; Yamashita et al., 2001), but a simple addition cannot remove systemic and motion artifacts that contribute to measured Δ[HbO] and Δ[HbR] with an equal sign.

This study exploits the hemoglobin covariation in fNIRS to dissociate multiple components and proposes a new analysis method that extracts task-related oxygenation and CBV changes by extending task-related component analysis (TRCA) that extracts task-related components (TRCs) as

a weighted linear sum of observed time courses. Our previous study demonstrated that TRCA was successfully applied to block-design and event-related synthetic data and fNIRS finger-tapping data (Tanaka et al., 2013). There, Δ[HbO] and Δ[HbR] were analyzed separately. Our analysis revealed two statistically significant TRCs: one with a localized map contralateral to tapping fingers, and the other with a rather uniform map over both hemispheres. Although their waveforms and maps differed clearly, a physiological interpretation of those components was not obvious in our previous paper. We thereby extend our previous method by taking into account the covariation of Δ[HbO] and Δ[HbR]. Based on Das' observation that oxygenation and CBV are reflected in the difference and the sum of Δ[HbO] and Δ[HbR], respectively (Sirotin and Das, 2009), this study extends the original TRCA by minimizing or maximizing the covariance between Δ[HbO] and Δ[HbR]. We first tested the extended TRCA with a synthetic data that was generated by a balloon model and found that task-related oxygenation and CBV changes could be reliably extracted. We then applied this analysis method to fNIRS data of both a motor task (finger tapping) and a cognitive task (spatial/verbal working memory) and found distinct time courses of oxygenation and blood volume, correspondingly with distinct spatial distributions. To investigate a phase relationship between oxygenation and CBV, phase plots of oxygenation and blood volume (or *"q-v"* plots) were drawn.

2. METHODS

2.1. Task-Related Component Analysis: A Formulation

Task-related components (TRCs) are constructed as a linear sum of original time courses of Δ[HbO] fNIRS channels ($\{x_{\mathrm{oxy},i}\}$, $i=1,\cdots,N$, N: the number of fNIRS channels) as

$$y_{\mathrm{oxy}}(t)=\sum_{i=1}^{N} w_i x_{\mathrm{oxy},i}(t)=\mathbf{w}^{\mathrm{T}}\mathbf{X}_{\mathrm{oxy}}(t), \tag{1}$$

and of Δ[HbR] channels ($\left\{x_{\mathrm{deoxy},i}\right\}$, $i=1,\cdots,N$) as

$$y_{\mathrm{deoxy}}(t)=\sum_{i=1}^{N} w_i x_{\mathrm{deoxy},i}(t)=\mathbf{w}^{\mathrm{T}}\mathbf{X}_{\mathrm{deoxy}}(t), \tag{2}$$

as depicted in Figure 1A. $\left\{x_{\mathrm{oxy},i}\right\}$ and $\left\{x_{\mathrm{deoxy},i}\right\}$ are normalized to zero mean and unit variance before taking the weighted sums. The same set of coefficients $\left\{w_i\right\}$ (or **w** in a vector form) is used both for Eqs. (1) and (2) so that y_{oxy} and y_{deoxy} are reconstructed from the same channel locations. TRCA in the original formulation optimizes the coefficients so that inter-block covariance between k- and l-th task blocks ($k,l=1,\cdots,K,\ k\neq l$, K: the number of task blocks) in y_{oxy}

$$C_{kl}^{\mathrm{OO}}=\mathrm{cov}\left(y_{\mathrm{oxy}}^{(k)}(t),y_{\mathrm{oxy}}^{(l)}(t)\right) \tag{3}$$

and in y_{deoxy}

$$C_{kl}^{\mathrm{DD}}=\mathrm{cov}\left(y_{\mathrm{deoxy}}^{(k)}(t),y_{\mathrm{deoxy}}^{(l)}(t)\right) \tag{4}$$

are maximized (Tanaka et al., 2013). Here $y_{\mathrm{oxy}}^{(k)}(t)$ and $y_{\mathrm{deoxy}}^{(k)}(t)$ denote k-th block segments of $y_{\mathrm{oxy}}(t)$ and $y_{\mathrm{deoxy}}(t)$, respectively. Note that, although a block-design experiment is used here, TRCA (and TRCA$^{\pm}$) is applicable both to block-design and event-related experiments as shown in (Tanaka et al., 2013).

Next, a covariation between Δ[HbO] and Δ[HbR] will be exploited to extract physiologically meaningful components. We first request that, in order to extract an oxygenation signal, y_{oxy} and y_{deoxy} be negatively correlated, so

$$C_{k}^{\mathrm{OD}}=\mathrm{cov}\left(y_{\mathrm{oxy}}^{(k)}(t),y_{\mathrm{deoxy}}^{(k)}(t)\right)\ \text{ and }\ C_{k}^{\mathrm{DO}}=\mathrm{cov}\left(y_{\mathrm{deoxy}}^{(k)}(t),y_{\mathrm{oxy}}^{(k)}(t)\right) \tag{5}$$

should take a minimal value, within each task block. The objective function to be maximized is defined as a sum of intra-Hb (C^{OO} and C^{DD}) and inter-Hb (C^{OD} and C^{DO}) covariances:

$$\sum_{\substack{k,l=1\\k\neq l}}^{K}\left(C_{kl}^{\mathrm{OO}}+C_{kl}^{\mathrm{DD}}\right)-\sum_{k=1}^{K}\left(C_{k}^{\mathrm{OD}}+C_{k}^{\mathrm{DO}}\right)=\mathbf{w}^{T}\mathbf{S}^{-}\mathbf{w}. \tag{6}$$

The coefficients that maximize this objective function should produce task-related oxygenation

changes whose Δ[HbO] and Δ[HbR] are negatively correlated. Similarly, we can consider TRCs whose Δ[HbO] and Δ[HbR] covary positively by maximizing the following objective function,

$$\sum_{\substack{k,l=1 \\ k\neq l}}^{K}\left(C_{kl}^{\mathrm{OO}}+C_{kl}^{\mathrm{DD}}\right)+\sum_{k=1}^{K}\left(C_{k}^{\mathrm{OD}}+C_{k}^{\mathrm{DO}}\right)=\mathbf{w}^{T}\mathbf{S}^{+}\mathbf{w}. \tag{7}$$

TRCs constructed with this objective function should reflect CBV changes associated with a current task. Here we assumed that task-related oxygenation changes and task-related CBV changes are characterized by negatively and positively correlated Δ[HbO] and Δ[HbR], respectively. This assumption holds in general (Sirotin and Das, 2009; Yamada et al., 2012); however, there are recent reports that certain changes in systemic factors such as speech induced hypocapnia and blood pressure can cause negatively correlated Δ[HbO] and Δ[HbR] (Scholkmann et al., 2013; Tachtsidis et al., 2009). This issue will be discussed in subsection 4.3 of Discussion.

These objective functions (Eqs (6) and (7)) are quadratic of **w** and thereby not bounded from above, so a proper constraint must be imposed for obtaining a meaningful solution. Similarly as in the original formulation of TRCA, we request that an averaged variance of y_{oxy} and y_{deoxy} be constrained to one as

$$\mathrm{Var}\left(y_{\mathrm{oxy}}(t)\right)+\mathrm{Var}\left(y_{\mathrm{deoxy}}(t)\right)=\mathbf{w}^{\mathrm{T}}\mathbf{Q}\mathbf{w}=1, \tag{8}$$

where the $N\times N$ matrix **Q** is defined as an average of covariance matrices of Δ[HbO] and of Δ[HbR]. Because $\left\{x_{\mathrm{oxy},i}\right\}$ and $\left\{x_{\mathrm{deoxy},i}\right\}$ are normalized to zero mean and unit variance and TRCs are normalized as in Eq. (8), TRCs are unitless. Therefore, in the following, "arbitrary unit (a.u.)" will be used for the labels of *y*-axis of TRCs. TRCA here is defined as maximization of either Eq. (6) or (7) under the constraint of Eq. (8). TRCA that minimizes (Eq. (6)) or maximizes (Eq. (7)) inter-Hb covariance will be referred to TRCA^{-} and TRCA^{+}, respectively, and these will be referred to $\mathrm{TRCA}^{\pm}$ collectively. This constrained maximization problem is equivalent to maximization of the

Rayleigh-Ritz quotient $\mathbf{w}^{\mathrm{T}}\mathbf{S}^{\pm}\mathbf{w} \big/ \mathbf{w}^{\mathrm{T}}\mathbf{Q}\mathbf{w}$, so solutions that maximize the quotient are given as

$$\hat{\mathbf{w}}^{\pm} = \arg\max_{\mathbf{w}} \frac{\mathbf{w}^{\mathrm{T}}\mathbf{S}^{\pm}\mathbf{w}}{\mathbf{w}^{\mathrm{T}}\mathbf{Q}\mathbf{w}}. \tag{9}$$

The solutions $\hat{\mathbf{w}}^{\pm}$ can be obtained as eigenvectors of $\mathbf{Q}^{-1}\mathbf{S}^{\pm}$, with corresponding eigenvalues $\lambda^{\pm}$. Corresponding TRCs are denoted by y^{+}_{oxy} and y^{+}_{deoxy} for $\hat{\mathbf{w}}^{+}$ and y^{-}_{oxy} and y^{-}_{deoxy} for $\hat{\mathbf{w}}^{-}$, respectively (Fig. 1B). These y^{+} and y^{-} should reflect task-related changes in blood volume and oxygenation, respectively. The components obtained with TRCA^{-} (y^{-}_{oxy} and y^{-}_{deoxy}) will be called task-related oxygenation changes, and the component obtained with TRCA^{+} (y^{+}_{oxy} and y^{+}_{deoxy}) will be called task-related CBV changes. The sign of eigenvectors cannot be determined by Eq. (9) *per se*, so we fix it so that correlation coefficients between y_{oxy} and $\mathbf{X}_{\mathrm{oxy}}$ and between y_{deoxy} and $\mathbf{X}_{\mathrm{deoxy}}$ are positive. Finally, the amplitudes of y^{+} and y^{-} are normalized to a unit variance. The MATLAB codes are available at the first author's website (http://www.jaist.ac.jp/~hirokazu/Site/Software.html).

2.2. Eigenvalue-Based Statistical Test

Eigenvalues in the previous subsection indicate the degree of reproducibility across task blocks and can thus be used for assessing their statistical significance of corresponding TRCs (Tanaka et al., 2013). A resampling-based test was used to assess statistical significance of $\lambda^{\pm}$ assuming a null hypothesis that there were no time courses that were significantly block-by-block reproducible. The distribution of eigenvalues was computed by uniformly randomizing the onsets of task blocks (null distribution), and the statistical significance of eigenvalues computed from the blocks actually used in experiments was assessed by comparing with the null distribution. This resampling-based statistical test was introduced in our previous paper and was found to be capable of testing the statistical significance. 200 times of the resampling procedure were iterated for obtaining the null

distribution. We set a 99% confidence interval reflecting a significance level of 0.01. Because we were interested in the most reproducible components of oxygenation and CBV changes, only the eigenvector with the largest eigenvalue in each session was used for further analyses if it was statistically significant. The oxygenation and the CBV changes that were significantly task-related found in individual subjects were then averaged, respectively.

The number of task blocks is an important experimental parameter that affects statistical significance of TRCs. Intuitively, the probability that the TRCA algorithm finds statistically significant TRCs should increase by including more task blocks. To test this intuition, we numerically computed the number of statistically significant TRCs by using initial n blocks of the working memory experiment (n ranging from 2 to 15).

2.3. Spatial Map

Spatial maps were constructed in order to quantify the spatial distributions of task-related oxygenation and CBV changes. Once TRCs were obtained, the oxy- and deoxy-hemoglobin spatial maps of individual subjects were constructed by computing a correlation coefficient between $y_{\mathrm{oxy}}(t)$ and $x_{\mathrm{oxy},i}(t)$ for the i-th Δ[HbO] channel and between $y_{\mathrm{deoxy}}(t)$ and $x_{\mathrm{deoxy},i}(t)$ for the i-th Δ[HbR] channel, respectively. Because the spatial maps were defined by correlation coefficients, their values ranged from zero to one and were unitless. These oxy- and deoxy-hemoglobin maps were then averaged to provide spatial maps of task-related oxygenation for TRCA^{-} and task-related CBV for TRCA^{+}. The spatial maps from all subjects were averaged to obtain the mean spatial map, referred to as the oxygenation and the CBV maps hereafter.

2.4. Synthetic Data Generated with Balloon Model

In order to test whether our method was capable of separating the oxygenation and CBV

changes, a balloon model composed of deoxy-Hb (q), blood volume (v) and total-Hb (p) was simulated as:

$$\begin{aligned}
\dot{q}(t) &= \frac{f_{\text{in}}(t)}{\tau_0}\left[\frac{E(t)}{E_0} - \frac{q(t)}{v(t)}\right] + \frac{1}{\tau_{\text{V}}}\left[f_{\text{in}}(t) - v^{1/\alpha}\right]\frac{q(t)}{v(t)}, \\
\dot{v}(t) &= \frac{1}{\tau_{\text{V}}}\left[f_{\text{in}}(t) - v^{1/\alpha}\right], \\
\dot{p}(t) &= \frac{1}{\tau_{\text{V}}}\left[f_{\text{in}}(t) - v^{1/\alpha}\right]\frac{p(t)}{v(t)}.
\end{aligned} \tag{10}$$

We used the same parameter values used in the previous publications (Cui et al., 2010; Mildner et al., 2001). The blood inflow $f_{\text{in}}(t)$ was modeled as a trapezoidal function with rise time 5 s, plateau time 15 s, decay time 5 s with plateau height 1.7. The oxygen extraction factor, E(t), was modeled as $E(t) = 1-(1-E_0)^{1/f_{\text{in}}(t)}$ where E_0 was 0.4. Other parameters were τ_0=2, τ_{v}=30, α=0.4. In the balloon model, Δ[HbO] is the difference between the total-Hb and deoxy-Hb, i.e., $p(t)$-$q(t)$. Ideally, Δ[HbO] and Δ[HbR] fNIRS channels should reflect $p(t)$-$q(t)$ and $q(t)$, respectively. Actually, however, fNIRS channels ($x_{\text{oxy},i}$ and $x_{\text{deoxy},i}$) contain not only oxygenation but also task-evoked blood volume changes. A recent study reported that fNIRS signals measured from the forehead was highly correlated with a sympathetic arterial vasoconstriction followed by a decrease in venous volume (Kirilina et al., 2012). We thus assumed that Δ[HbO] and Δ[HbR] channels were mixtures of $p(t)$-$q(t)$, $q(t)$, $v(t)$ and some systemic and motion artifacts, and four artificial time courses were simulated for oxy and deoxy fNIRS channels:

$$\begin{aligned}
\mathbf{X}_{\text{oxy}} &= \begin{pmatrix} x_{\text{oxy},1} & x_{\text{oxy},2} & x_{\text{oxy},3} & x_{\text{oxy},4} \end{pmatrix}^T = \mathbf{A}\mathbf{R}_{\text{oxy}}, \\
\mathbf{X}_{\text{deoxy}} &= \begin{pmatrix} x_{\text{deoxy},1} & x_{\text{deoxy},2} & x_{\text{deoxy},3} & x_{\text{deoxy},4} \end{pmatrix}^T = \mathbf{A}\mathbf{R}_{\text{deoxy}}.
\end{aligned} \tag{11}$$

Here, four dimensional vectors, $\mathbf{R}_{\text{oxy}}$ and $\mathbf{R}_{\text{deoxy}}$, were defined as

$$\begin{aligned}
\mathbf{R}_{\text{oxy}} &= \begin{pmatrix} p(t)-q(t) & v(t) & n_{\text{Mayer}}(t) & n_{\text{motioin}}(t) \end{pmatrix}^T, \\
\mathbf{R}_{\text{deoxy}} &= \begin{pmatrix} q(t) & v(t) & n_{\text{Mayer}}(t) & n_{\text{motion}}(t) \end{pmatrix}^T.
\end{aligned} \tag{12}$$

and **A** denotes a mixing matrix. *p*, *q*, and *v* in the first two components in $\mathbf{R}_{\text{oxy}}$ and $\mathbf{R}_{\text{deoxy}}$ are the total-Hb, deoxy-Hb, and the blood volume derived from the balloon model, and n^{Mayer} and n^{motion}. fNIRS signals contain artifacts originating from cardiac pulsations (Obrig et al., 2002; Strangman et al., 2002; Taga et al., 2000) and from body motion (Cooper et al., 2012; Sato et al., 2006), and the last two components in $\mathbf{R}_{\text{oxy}}$ and $\mathbf{R}_{\text{deoxy}}$ were synthetic artifacts mimicking the Mayer wave and body motion, respectively. We note that details in the synthetic artifacts were not important as the TRCA algorithm is able to remove these artifacts unless they happen to coincide with task onsets (Tanaka et al., 2013). The Mayer wave was modeled as a sinusoidal wave of period 12 seconds whose amplitude was modulated by a slow oscillation of period 180 seconds, and the body motion artifact was modeled as a sum of exponentially decay functions whose amplitudes and time constants were randomized. In a given fNIRS channel (i.e., $x_{\text{oxy},i}$ and $x_{\text{deoxy},i}$), the oxygenation and the blood volume were assumed to be mixed with fixed coefficients, and the Mayer-wave and motion artifacts contributed equally to $x_{\text{oxy},i}$ and $x_{\text{deoxy},i}$, as summarized in Eq. (11). To create synthetic data, the following values for components of the mixing matrix were used:

$$\mathbf{A} = \begin{pmatrix} 0.3 & 1.2 & -0.8 & 0.8 \\ 0.6 & 0.9 & 0.8 & -0.8 \\ 0.9 & 0.6 & 0.8 & -0.8 \\ 1.2 & 0.3 & -0.8 & 0.8 \end{pmatrix}. \tag{13}$$

With this mixing matrix, x_1, for example, was a mixture of oxygenation and blood volume at a one-to-four ratio, and x_4 was at a four-to-one ratio. x_2 and x_3 contained oxygenation and blood volume more or less equally. x_1 and x_4 contained negative and positive contributions of the Mayer wave and motion artifact, respectively, and x_2 and x_3 vice versa. In addition, independent Gaussian noise with a variance of 0.2^2 was added to $\mathbf{X}_{\text{oxy}}$ and $\mathbf{X}_{\text{deoxy}}$. The simulation result was not sensitive to the particular choice of the mixing matrix (Eq. (13)) or the degree of Gaussian noise; we reiterated the same simulation by randomizing the values of mixing matrix or increasing the noise level, and

verified the robustness of the results, as long as the mixing matrix was not close to singular.

2.5. Construction of *q*-*v* plot from experimental data

To describe relative timings of oxygenation and CBV changes, a phase plot of total deoxy-hemoglobin (*q* in the balloon model) and blood volume (*v*), called *q*-*v* plot, is often used (Buxton et al., 2004; Toyoda et al., 2008). Clockwise and counter-clockwise curves in a *q*-*v* plot suggest a phase lead of oxygenation and blood volume, respectively, and the area surrounded by a curve represents the degree of phase difference (i.e., perfectly synchronized hemoglobin and blood volume gives a zero area). y^{-}_{deoxy} of TRCA^{-} is regarded as (unnormalized) task-related deoxy-hemoglobin concentration change, and y^{+}_{oxy} and y^{+}_{deoxy} of TRCA^{+} reflect (unnormalized) task-related blood volume change. Therefore, we used y^{-}_{deoxy} for the *q* variable and average of y^{+}_{oxy} and y^{+}_{deoxy} for the *v* variable and plotted transient changes in the two-dimensional *q*-*v* plane.

2.6. fNIRS Finger-Tapping Experiment

Twenty-nine subjects participated in two sessions of the finger-tapping experiment: one session with right fingers and the other with left fingers (for the experimental details, see (Sato et al., 2005)). Single experimental sessions consisted of five task blocks of 30 seconds interleaved with rest periods of 30 seconds. Twenty-four fNIRS channels (ETG-100, Hitachi Medical Corporation, Japan) were placed over 6×6 cm areas of the left and right sensorimotor areas (twelve channels on each hemisphere) centered at C3 and C4 positions, respectively. The source-detector distance was 30 mm, and the fNIRS signals were sampled at 10 Hz. Before applying TRCA, the whole time courses of fNIRS signals were moving averaged for one second and detrended using 6-th order polynomials. This data set was analyzed in our previous publications (Katura et al., 2008; Sato et al., 2005; Tanaka et al., 2013). As in our previous publication, 5 seconds before the task-block onset and 20 seconds

after the task-block end were included for computing the inter-block covariances, so the total duration used for TRCA was 55 seconds.

2.7. fNIRS Working-Memory Experiments

Seventeen subjects participated in three sessions of a spatial WM experiment and in other three sessions of a verbal WM experiment, totally six sessions each subject. Presented stimuli to remember were white squares at randomly chosen locations for the spatial WM experiment or Japanese characters at prefixed locations for the verbal WM experiment. This data set was used for our previous study with experimental details described therein (Sato et al., 2011). Each session consisted of 16 task blocks with 10.5 second duration; a brief stimulus presentation period (1.5 seconds), the maintenance period (7.0 seconds), and the retrieval period (2.0 seconds). Of these task blocks, two stimuli were presented in a half of the blocks and four in the other half, and the order of two- and four-item blocks was randomized on a subject-by-subject basis. We included both two- and four-item blocks for the analysis. The fNIRS signals were measured using ETG-7100 (Hitachi Medical Corporation). Fifteen sources and fifteen detectors were placed over the prefrontal cortex in a 3×10 lattice pattern, and each source-detector pair was separated by 30 mm, thereby providing 47 measurement channels (for channel positions, see Figs. 6C, 6D, 7C and 7D). The fNIRS signals were preprocessed by moving-averaging over one second and detrending with 6-th order polynomials over the entire time courses. To apply TRCA, 5 seconds before and 14.5 seconds after the block were included, so totally 30 seconds were used for TRCA. We used all the task blocks except the last one because the measurement did not include 14.5 seconds after the last task block.

3. RESULTS

3.1. Balloon Model Simulation

Time courses of oxy-Hb, deoxy-Hb, and CBV changes were simulated with the balloon model equations (Eq. (10)) along with the Mayer-wave and motion artifacts (Fig. 2A), and synthetic fNIRS time courses were created by mixing the results of balloon model with the artifacts (Eqs. (11) and (12)) (Fig. 2B) (See Section 2.4). From a visual inspection, channel 1 (x_1) contained positively correlated Δ[HbO] and Δ[HbR] and channel 4 (x_2) contained negatively correlated Δ[HbO] and Δ[HbR], but it was not apparent that these were composed of Δ[HbO] ($p(t)$-$q(t)$), Δ[HbO] ($q(t)$), and the CBV ($v(t)$) time courses generated by simulating the balloon model equations in Figure 2A. TRCA$^{\pm}$ was capable of recovering the volume and oxygenation time courses; TRCA^{+} recovered the CBV course (normalized $v(t)$ in the balloon model) (Fig. 2C), and TRCA^{-} recovered the oxy-Hb (normalized $p(t)$-$q(t)$) and the deoxy-Hb (normalized $q(t)$) (Fig. 2D). These results demonstrated that TRCA can extract both the blood volume and the oxygenation simultaneously, provided that fNIRS signals reflect the changes of both oxygenation and blood volume.

To see the temporal development of dynamical variables in the balloon model, a phase plot of $q(t)$ and $v(t)$ (or q-v plot) is often depicted (Buxton et al., 2004; Toyoda et al., 2008). Here the TRCs corresponding to $q(t)$ and $v(t)$ were y^{-}_{deoxy} and y^{+}_{deoxy}, respectively, so we reconstructed a phase plot using y^{-}_{deoxy} from Fig. 2D and y^{+}_{deoxy} from Fig. 2C (Fig. 2E). The simulation result suggests that TRCA$^{\pm}$ can extract the oxygenation and CBV changes from noisy and mixed measurements, and we proceeded to apply TRCA$^{\pm}$ to the fNIRS data of finger-tapping and working-memory experiments, as explained below.

3.2. fNIRS Data of Finger-Tapping Experiment

There were 23 and 27 statistically significant TRCs found by TRCA^{-} and TRCA^{+}, respectively,

from the 29-subject fNIRS data set of the right finger-tapping experiment (Sato et al., 2005) depicted in Figures 3A and 3C. The oxygenation time courses (y^{-}_{oxy} and y^{-}_{deoxy}) obtained in TRCA^{-} showed a gradual increase and decrease immediately after the task-block onset and subsequently a gradual decay following the task-block end, showing the characteristic of a typical hemodynamic response function (red and black lines in Fig. 3A). On the contrary, the CBV time courses (y^{+}_{oxy} and y^{+}_{deoxy}) obtained in TRCA^{+} were quite distinct from those of oxygenation: a linear increase during the rest period until the peak about five seconds after the task onset, followed by a gradual decline during the task period (red and black lines in Fig. 3C). The corresponding spatial maps differed between TRCA$^{\pm}$; the oxygenation map was found mainly in the ventral part of contra-lateral sensorimotor area (Fig. 3B), whereas the CBV map showed high values in the dorsal part of contra-lateral sensorimotor area (Fig. 3D). Similar results were obtained for the left finger-tapping experiment (27 and 23 statistically significant TRCs, respectively for TRCA^{-} and TRCA^{+}) (Fig.4). The time courses of $y^{\pm}_{\mathrm{oxy}}$ resembled those reported in our previous study; a gradually changing component and a piece-wise linear component (Tanaka et al., 2013).

Figure 5 summarized block averages of task-related oxygenation and CBV changes, respectively (Panels A and B for right fingers and Panels D and E for left fingers). The time courses of oxygenation (solid lines) and CBV (broken lines) differed distinctively on their rise and decay shapes. To examine their transient dynamics, we plotted the trajectory of y^{-}_{deoxy} and y^{+}_{deoxy} (Figs. 5C and 5F). These plots indicate the faster rise at the task onset and the larger undershoot after the task end in CBV in comparison with oxygenation.

3.3. fNIRS Data of Working-Memory Experiment

TRCA$^{\pm}$ was then applied to fNIRS data of the spatial and verbal WM experiments (Sato et al., 2011). For both TRCA^{+} and TRCA^{-}, there were 51 statistically significant components from the

three-session data of 17 subjects (thereby 51 independent sessions). To investigate how the number of task blocks influenced the number of statistically significant TRCs, we iterated the statistical test by using initial *n* blocks out of the total 15 blocks (*n* ranging from 2 to 15). When only initial two blocks were used, about 40% of sessions yielded statistically significant components. The number of statistically significant components increased almost monotonically with more number of task blocks, and got saturated at around 12 task blocks.

For verbal WM, Figure 6A depicts the oxygenation time courses (y^{-}_{oxy} (red) and y^{-}_{deoxy} (black)), and Figure 6B depicts the CBV time courses (y^{+}_{oxy} (red) and y^{+}_{deoxy} (black)). The oxygenation map showed high values of correlation coefficients around the dorsolateral prefrontal cortex (Fig. 6C), whereas the CBV map appeared significantly in the ventral prefrontal cortex (Fig. 6D). Similar results were obtained for spatial WM (Figs 7A and 7B) and the corresponding oxygenation and CBV maps (Figs. 7C and 7D).

To examine these time courses more closely, block averages were computed. Figure 8 shows block averages of the time courses in Figures 6 and 7. The time courses of y^{-}_{oxy} and y^{+}_{oxy} were almost same but there was a slight phase lead of y^{+}_{oxy} over y^{-}_{oxy} (Figs. 8A and 8D), so cross correlation was computed for 15 blocks in order to assess the phase difference. The lag between y^{-}_{oxy} and y^{+}_{oxy} was defined, by a block-by-block basis, as the time difference that maximized the cross correlation between both time courses. We defined that a positive (negative) lag meant a phase lead of y^{+}_{oxy} (y^{-}_{oxy}). The lag was positive both for verbal (mean 0.78 (s), SD 0.60 (s)) and spatial (mean 1.03 (s), SD 0.95 (s)) WM, and was significantly different from zero (one-sided *t*-test, $p=9.7\times10^{-5}$ for verbal and $p=4.3\times10^{-4}$ for spatial WM). This result implies that the rise of CBV change was about one second earlier than that of oxygenation change in the WM experiments. Phase plots between y^{-}_{deoxy} and y^{+}_{deoxy} were constructed (Figs. 8C and 8F), confirming the earlier rise and decay of CBV compared with those of oxygenation.

4. DISCUSSION

Based on TRCA that maximizes inter-block covariances of Δ[HbO] or Δ[HbR] separately, this study proposed an analysis method (TRCA$^{\pm}$) that estimates task-related oxygenation and CBV changes by exploiting the covariation between Δ[HbO] and Δ[HbR]. TRCA$^{\pm}$ was tested with synthetic data generated by simulating a balloon model, successfully recovering task-related oxygenation and CBV changes. We then analyzed the fNIRS data sets of finger-tapping and working-memory tasks and found distinct time courses and spatial distributions for oxygenation and CBV changes. We provide a concrete physiological interpretation of the two components found in the finger-tapping experiment reported before. The merit of this analysis method is that it is applicable to reanalysis of existing data sets. We believe that TRCA$^{\pm}$ extends the applicability of fNIRS to a number of applications, such as understanding of the mechanisms of neurovascular coupling (Obrig et al., 2002; Wolf et al., 2002), validation of balloon-model processes (Huppert et al., 2006; Steinbrink et al., 2006), and monitoring of cerebrovascular hemodynamics in stroke patients (Kim et al., 2010; Saitou et al., 2000).

Conventionally, CBV changes are estimated from total hemoglobin (i.e., Δ[HbO]+ Δ[HbR]) (Wyatt et al., 1990), and oxygenation changes are estimated from a difference of oxy- and deoxy-hemoglobin (i.e., Δ[HbO]- Δ[HbR]) (Wyatt et al., 1986). But, a merely summing or subtracting Δ[HbO] and Δ[HbR] cannot remove systemic and motion artifacts, which contribute significantly to oxy- and deoxy-hemoglobin fNIRS channels. TRCA$^{\pm}$ circumvents this issue by requiring the reproducibility over task blocks, which can remove task-unrelated artifacts as shown in our previous work (Tanaka et al., 2013). We conclude that TRCA$^{\pm}$, unlike most extant analysis methods, exploits the hemoglobin covariance to extract the task-related oxygenation and CBV, making the best use of the fNIRS advantage of simultaneous Δ[HbO]-Δ[HbR] measurement.

TRCA here was formulated using a weighted linear sum in Eqs. (1-2). Weighted linear summation is a simple yet most commonly used method for signal processing as in principle component analysis (PCA), independent component analysis (ICA), and linear discriminant analysis (LDA). A linear sum does not necessarily imply that all channels show a same effect because, if there is a component that is localized in space, the corresponding weights should reflect its locality. We note that a weighted linear sum is an approximation and may be extended to some nonlinear methods. Our formulation of TRCA shares its mathematical form with those of PCA and LDA, which have been extended to a nonlinear, kernel-based version (Mika et al., 1999a; Mika et al., 1999b). TRCA may hence be extended to a kernel-based algorithm. Also, the linear sums with constant coefficients over the whole time series (Eqs. (1-2)) implicitly assumes that TRCs contribute to fNIRS channels in a static manner. This assumption is likely to hold for experiments of short duration but is likely violated for experiments long enough to induce subjects' fatigue or learning or to involve changes in contacts between scalp and optodes. One possible solution is to develop an online, recursive algorithm for TRCA that accommodates such time-dependent changes, as developed in LDA (Hiraoka et al., 2000) and ICA (Akhtar et al., 2012). It would be interesting to formulate kernel-based and online versions of TRCA and to investigate how the performance will be improved.

4.1. Relation to the Balloon model

There are two general approaches to characterizing the transformation from neural activities hemodynamic responses measured in neuroimaging. One approach is to model physiologically detailed processes connecting neural activities to hemodynamic changes. Blood oxygen-level dependent (BOLD) signals elicited by presented stimuli, together with CBV, cerebral blood flow (CBF), oxygen extraction factor (OEF) and oxygenation, have been modeled as a balloon model,

which reproduces a number of the key characteristics of BOLD signals quantitatively (Buxton et al., 2004; Buxton et al., 1998; Mildner et al., 2001). The balloon model has been tested and verified by using simultaneous imaging measurements such as fMRI and fNIRS (Huppert et al., 2006; Steinbrink et al., 2006; Toyoda et al., 2008). An alternative approach is a phenomenological approach that describes an input-output relation. BOLD signals have been modeled as an impulse-response-function model, without considering physiological processes (Boynton et al., 1996; Soltysik et al., 2004).

Our results have shown that, by constructing phase *q*-*v* plots, the phase differences between oxygenation and CBV changes were determined; specifically, the rise of CBV was earlier than that of oxygenation in our data sets of the finger-tapping and working-memory tasks, thereby providing certain constraints on the balloon-model parameters. The proposed method is advantageous in examining the phase difference between oxygenation and CBV changes because it requires only a normal fNIRS instrument, without combining with other measurement modalities. We plan to conduct a systematic study that compares the oxygenation-CBV dynamics for a variety of sensory, motor and cognitive tasks and optimize the balloon model parameters that best explains the experimental data.

4.2. Oxygenation and CBV Time Courses and Spatial Distributions

By analyzing Δ[HbO] of the finger-tapping experiment our previous paper reported a gradually changing component a piece-wise linear component with distinct spatial distributions (Fig. 9 for right fingers and Fig. 10 for left fingers in (Tanaka et al., 2013)). Our putative interpretation then was that the gradually changing component represented a hemodynamic response due to its contralateral localization whereas the piece-wise linear component reflected systemic activities due to its bilateral distribution. TRCA$^{\pm}$, by taking both Δ[HbO] and Δ[HbR], found components that resembled those

reported in our previous paper. The gradually changing components had a negative Δ[HbO]-Δ[HbR] covariance whereas the piece-wise linear component had a positive Δ[HbO]-Δ[HbR] covariance, indicating that the former and the latter can be interpreted as oxygenation and CBV, respectively. These components differed in three aspects: the shapes of their time courses, the spatial distributions, and the Δ[HbO]-Δ[HbR] covariance.

Our new analysis in this report revealed a difference between the spatial distributions of oxygenation and CBV changes both in the finger-tapping and the WM data. In the finger tapping data, the CBV map was more wide spread over both hemispheres whereas the oxygenation map was more concentrated in the hemisphere contralateral to the tapping fingers. In the WM data, the CBV map had a high value in the ventral prefrontal area whereas the oxygenation map in the dorsolateral prefrontal areas in both hemispheres. (Sirotin et al., 2012) reported that a blood volume component measured with a green light (an isobet) was homogeneous in the imaged area (10 mm × 10 mm) and was not predicted by concurrently recorded spiking or local field potentials.

q-v plots provide a succinct summary of phase difference between oxygenation and CBV changes. Whereas the results for both the finger-tapping and the working-memory experiments demonstrated a phase lead of the CBV changes over the oxygenation changes, the degree of phase lead appeared more considerable for the finger-tapping experiment than that in the working-memory experiment. This difference can be traced back to the distinct temporal shapes of the CBV changes (Figures 3C and 4C for finger tapping and Figures 6B & 7B for working memory). We speculate that the CBV changes might be more susceptible to systemic factors such as blood pressure, which could be modulated in motor tasks more than in cognitive tasks.

The CBV change in the balloon model attributed in response to stimulus presentation and thus appears only after the onset of stimuli. Both the presumed blood volume signals found in the finger-tapping experiment and the anticipatory signals measured with green light in Das' studies,

however, cannot be explained by a current formulation of the balloon model because those signals change during rest periods in which no sensory stimuli or motor outputs were involved. Moreover, we found that the spatial distributions of oxygenation and CBV changes differed, in consistent with the results from Das' group, which cannot be accounted for by the balloon model where all variables interact at a single point. These results as a whole indicate that the balloon model be revised substantially.

With the abovementioned arguments, we would like to posit that oxygenation and CBV components derived with $TRCA^{\pm}$ might correspond to the stimulus-related and task-related components, respectively, reported in the intrinsic optical imaging of monkeys. To test the hypothesis that task-related and stimulus-related components might be measurable non-invasively from human subjects, a preliminary experiment was conducted. Nine subjects performed a finger-tapping task with a fixed task period (30 s) and a variable rest period (20 or 40 s). We found that time courses of $TRCA^{-}$ were almost invariant regardless of a short or long period of rest, indicating that these components were related only to motor execution. On the other hand, time courses of $TRCA^{+}$ changed their periodicity entrained to the change of rest period, indicating that these components reflected the structure of the task including both task and rest periods. We will report these findings in our forthcoming paper (Tanaka et al. in preparation).

4.3. Limitations

Although the positive or negative covariation between Δ[HbO] and Δ[HbR] is a prerequisite for a measure for oxygenation and CBV, the covariation itself doesn't guarantee that those fNIRS signals have a cortical origin. There is a recent concern that fNIRS signals contain not only cortical hemodynamic responses resulting from neural activities but also extracranial hemodynamic changes in the soft tissues such as skins (Takahashi et al., 2011) and veins draining the scalp (Kirilina et al.,

2012). Extracranial hemodynamic changes tend to have positively correlated Δ[HbO] and Δ[HbR] (Yamada et al., 2012), so it is possible that the TRCs derived by $TRCA^+$ contain not only CBV but also certain extracranial signals. Indeed, our recent study of simultaneous fNIRS-fMRI recording has found that, during a working memory task, Δ[HbO] in the ventral prefrontal area showed a high correlation with not only cortical BOLD signals measured with fMRI but also superficial blood flow measured with a laser Doppler flowmeter (Sato et al., 2013). Care should be taken, therefore, before concluding that CBV changes derived by $TRCA^+$ originate from the gray matter. In such case, the time courses of extracranial and cortical origins are highly correlated, so signal processing methods such as one proposed in the report *per se* cannot conclude their physiological origin. One possible solution is to integrate signal processing methods with an fNIRS measurement with multiple-distance optodes (Funane et al., 2013), where a pair of short- and long-distance optodes quantify signals from a shallow and a deep tissue layer, respectively.

It is also possible that the TRCs derived by $TRCA^-$ contain not only cortical oxygenation but also non-cortical, systemic signals. There are recent papers reporting negatively correlated Δ[HbO] and Δ[HbR] that were induced by changes in speech associated end-tidal CO_2 (Scholkmann et al., 2013) or blood pressure (Tachtsidis et al., 2009). (Scholkmann et al., 2013) reported that speech-related hyper-ventilation led to hypocapnia (a decrease in oxy-Hb concentration and an increase in deoxy-Hb concentration), whereas the TRCs by $TRCA^-$ contained a positive and a negative change in Δ[HbO] and Δ[HbR], respectively. Therefore, for the finger-tapping and working-memory tasks, the effects of end-tidal CO_2 appear to be minimal. In contrast, in an anagram task, a change in blood pressure correlated positively with Δ[HbO] and negatively with Δ[HbR], so an increase in Δ[HbO] and a decrease in Δ[HbR] may result from systemic factors. To conclude, systemic variables should be monitored simultaneously in order to correctly interpret fNIRS signals, as emphasized by (Kirilina et al., 2013; Scholkmann et al., 2013; Tachtsidis et al., 2009).

There are two main approaches in neuroimaging data analysis; one is hypothesis driven represented by general linear models (GLM) (Friston et al., 1994; Minagawa-Kawai et al., 2011), and another is data driven represented by ICA (Makeig et al., 1996; McKeown and Sejnowski, 1998). The comparison of TRCA with the two approaches was made in our previous paper (Tanaka et al., 2013). We note that analysis methods based on trial average in time domain including TRCA cannot detect some components that are oscillatory and not phase locked to task onsets. These non phase-locked components may be detectable by using ICA (Makeig et al., 2002). We suggest to apply multiple, complementary analysis methods for a better understanding of neuroimaging data.

Acknowledgments

It is our pleasure to thank Drs. Norihiro Sadato, Masashi Kiguchi, Kenji Ogawa and Hiroshi Imamizu for their valuable comments on the interpretation of fNIRS signals, and Dr. Terrence J. Sejnowski for comments on the comparison with ICA and TRCA. We are indebted to Dr. Isao Nambu for his comments on the manuscript and Mr. Takanori Sato for his assistance in improving the analysis code. The simulation code of the balloon model was kindly provided by Dr. Xu Cui. Finally, we thank two anonymous reviewers for the helpful comments, which improved the manuscript considerably.

Figure Legends

Figure 1. (A) Schematics of TRCA. y_{oxy} and y_{deoxy} are constructed by a linear sum of $\mathbf{X}_{\text{oxy}}$ and $\mathbf{X}_{\text{deoxy}}$, respectively, and inter-block covariances within $y_{\text{oxy}}^{(k)}$ (C^{OO}) and within $y_{\text{deoxy}}^{(l)}$ (C^{DD}) are maximized. In addition, inter-hemoglobin covariance between $y_{\text{oxy}}^{(k)}$ and $y_{\text{deoxy}}^{(k)}$ (C^{OD} and C^{DO}) is minimized for extracting an oxygenation change or maximized for extracting a CBV change. (B) Illustrative example of TRCA$^{\pm}$. TRCA^{+} constructs CBV components (y_{oxy}^{+} and y_{deoxy}^{+}), and TRCA^{-} constructs oxygenation components (y_{oxy}^{-} and y_{deoxy}^{-}). The data in the left was from a subject performing left finger tapping.

Figure 2. Reconstruction of CBV and oxygenation changes synthesized with a balloon model. (A) Synthetic time courses of oxygenation (oxy- and deoxy-Hb), CBV, and artifacts (the Mayer wave and body motion). (B) Simulated observed data ($x_{\text{oxy},i}$ and $x_{\text{deoxy},i}$). (C) Reconstructed CBV change by TRCA^{+} and (D) oxygenation change by TRCA^{-}. The red and blue solid lines depict y_{oxy}^{+} and y_{deoxy}^{+}, respectively, in (C), and y_{oxy}^{-} and y_{deoxy}^{-}, respectively, in (D). The black dashed lines depict the corresponding model CBV and oxygenation changes, respectively, in (C) and (D) (normalized to zero mean and unit variance for a comparison). (E) *q*-*v* phase plot of y_{deoxy}^{-} and y_{deoxy}^{+}.

Figure 3. Time courses of (A) task-related oxygenation and (B) task-related CBV changes constructed from right finger-tapping data. The blue shaded areas indicate task periods of 30 seconds interleaved with rest periods of 30 seconds. The red and black solid lines depict y_{oxy} and y_{deoxy}, respectively, accompanied with shaded color areas of standard errors. Corresponding (C) oxygenation and (D) CBV maps. Colors in the maps represent

correlation coefficients averaged over all subjects.

Figure 4. Results of left-finger tapping in the same format of Figure 3.

Figure 5. Block averages of oxy- (y^{-}_{oxy} and y^{+}_{oxy} for (A) right tapping and (D) left tapping) and deoxy-Hb (y^{-}_{deoxy} and y^{+}_{deoxy} for (B) right tapping and (E) left tapping). Time courses obtained by TRCA^{-} and TRCA^{+} are denoted by the solid and dashed lines, respectively. The error bars accompanying the time courses indicate standard errors. *q*-*v* phase plots of the deoxy-signals are shown in (C) for right tapping and in (F) for left tapping. The gray circles indicate the starting positions, and the arrows are placed in steps of two seconds.

Figure 6. (A) Task-related oxygenation and (B) task-related CBV changes found in the spatial WM experiment. The red and black solid lines represent y_{oxy} and y_{deoxy}, respectively, along with standard errors indicated by the shaded areas. The blue shaded areas are the task periods of 10 seconds stating with the onset of stimulus presentation. Spatial maps for (C) oxygenation and (D) CBV changes.

Figure 7. Results of the verbal WM experiment in the format of Figure 6.

Figure 8. Block averages of task-related oxy-hemoglobin (y^{-}_{oxy} and y^{+}_{oxy} for (A) verbal and (D) spatial WM) and deoxy-hemoglobin (y^{-}_{deoxy} and y^{+}_{deoxy} for (B) verbal and (E) spatial WM). The solid and dashed lines denote the task-related oxygenation and CBV changes, respectively. The error bars accompanying the time courses indicate standard errors. Phase plots are shown for (C) the verbal and in (F) spatial WM tasks. The gray circles indicate the starting positions, and the arrows are placed in steps of one second.

References

Akhtar, M.T., Jung, T.-P., Makeig, S., Cauwenberghs, G., 2012. Recursive independent component analysis for online blind source separation. Circuits and Systems (ISCAS), 2012 IEEE International Symposium on. IEEE, pp. 2813-2816.

Boynton, G.M., Engel, S.A., Glover, G.H., Heeger, D.J., 1996. Linear systems analysis of functional magnetic resonance imaging in human V1. The Journal of Neuroscience 16, 4207.

Buxton, R.B., Uludag, K., Dubowitz, D.J., Liu, T.T., 2004. Modeling the hemodynamic response to brain activation. NeuroImage 23 Suppl 1, S220-233.

Buxton, R.B., Wong, E.C., Frank, L.R., 1998. Dynamics of blood flow and oxygenation changes during brain activation: the balloon model. Magn Reson Med 39, 855-864.

Cardoso, M.M., Sirotin, Y.B., Lima, B., Glushenkova, E., Das, A., 2012. The neuroimaging signal is a linear sum of neurally distinct stimulus- and task-related components. Nat Neurosci 15, 1298-1306.

Cooper, R.J., Selb, J., Gagnon, L., Phillip, D., Schytz, H.W., Iversen, H.K., Ashina, M., Boas, D.A., 2012. A systematic comparison of motion artifact correction techniques for functional near-infrared spectroscopy. Front Neurosci 6, 147.

Cui, X., Bray, S., Reiss, A.L., 2010. Functional near infrared spectroscopy (NIRS) signal improvement based on negative correlation between oxygenated and deoxygenated hemoglobin dynamics. NeuroImage 49, 3039-3046.

Devor, A., Dunn, A.K., Andermann, M.L., Ulbert, I., Boas, D.A., Dale, A.M., 2003. Coupling of total hemoglobin concentration, oxygenation, and neural activity in rat somatosensory cortex. Neuron 39, 353-359.

Friston, K.J., Holmes, A.P., Worsley, K.J., Poline, J.P., Frith, C.D., Frackowiak, R.S.J., 1994. Statistical parametric maps in functional imaging: a general linear approach. Hum Brain Map 2, 189-210.

Funane, T., Atsumori, H., Katura, T., Obata, A.N., Sato, H., Tanikawa, Y., Okada, E., Kiguchi, M., 2013. Quantitative evaluation of deep and shallow tissue layers' contribution to fNIRS signal using multi-distance optodes and independent component analysis. NeuroImage.

Hiraoka, K., Yoshizawa, S., Hidai, K.-i., Hamahira, M., Mizoguchi, H., Mishima, T., 2000. Convergence analysis of online linear discriminant analysis. Neural Networks, 2000. IJCNN 2000, Proceedings of the IEEE-INNS-ENNS International Joint Conference on. IEEE, pp. 387-391.

Huppert, T.J., Hoge, R.D., Diamond, S.G., Franceschini, M.A., Boas, D.A., 2006. A temporal comparison of BOLD, ASL, and NIRS hemodynamic responses to motor stimuli in adult humans. NeuroImage 29, 368-382.

Katura, T., Sato, H., Fuchino, Y., Yoshida, T., Atsumori, H., Kiguchi, M., Maki, A., Abe, M., Tanaka, N., 2008. Extracting task-related activation components from optical topography measurement using independent components analysis. Journal of biomedical optics 13, 054008.

Katura, T., Tanaka, N., Obata, A., Sato, H., Maki, A., 2006. Quantitative evaluation of interrelations between spontaneous low-frequency oscillations in cerebral hemodynamics and systemic cardiovascular dynamics. NeuroImage 31, 1592-1600.

Kim, M.N., Durduran, T., Frangos, S., Edlow, B.L., Buckley, E.M., Moss, H.E., Zhou, C., Yu, G., Choe, R., Maloney-Wilensky, E., Wolf, R.L., Grady, M.S., Greenberg, J.H., Levine, J.M., Yodh, A.G., Detre, J.A., Kofke, W.A., 2010. Noninvasive measurement of cerebral blood flow and blood oxygenation using near-infrared and diffuse correlation spectroscopies in critically brain-injured adults. Neurocrit Care 12, 173-180.

Kirilina, E., Jelzow, A., Heine, A., Niessing, M., Wabnitz, H., Bruhl, R., Ittermann, B., Jacobs, A.M., Tachtsidis, I., 2012. The physiological origin of task-evoked systemic artefacts in functional near infrared spectroscopy. NeuroImage 61, 70-81.

Kirilina, E., Yu, N., Jelzow, A., Wabnitz, H., Jacobs, A.M., Tachtsidis, I., 2013. Identifying and quantifying main components of physiological noise in functional near infrared spectroscopy on the prefrontal cortex. Frontiers in Human Neuroscience 7, 864.

Kohno, S., Miyai, I., Seiyama, A., Oda, I., Ishikawa, A., Tsuneishi, S., Amita, T., Shimizu, K., 2007. Removal of the skin blood flow artifact in functional near-infrared spectroscopic imaging data through independent component analysis. J Biomed Optics 12, 062111.

Makeig, S., Bell, A.J., Jung, T.P., Sejnowski, T.J., 1996. Independent component analysis of electroencephalographic data. Advances in Neural Information Processing Systems, 145-151.

Makeig, S., Westerfield, M., Jung, T.P., Enghoff, S., Townsend, J., Courchesne, E., Sejnowski, T.J., 2002. Dynamic brain sources of visual evoked responses. Science 295, 690-694.

Malonek, D., Grinvald, A., 1996. Interactions between electrical activity and cortical microcirculation revealed by imaging spectroscopy: implications for functional brain mapping. Science 272, 551-554.

Mayhew, J., Zheng, Y., Hou, Y., Vuksanovic, B., Berwick, J., Askew, S., Coffey, P., 1999. Spectroscopic analysis of changes in remitted illumination: the response to increased neural activity in brain. NeuroImage 10, 304-326.

McKeown, M.J., Sejnowski, T.J., 1998. Independent component analysis of fMRI data: examining the assumptions. Human brain mapping 6, 368-372.

Mika, S., Ratsch, G., Weston, J., Scholkopf, B., Mullers, K.R., 1999a. Fisher discriminant analysis with kernels. Neural Networks for Signal Processing IX: Proceedings of the 1999 IEEE Signal Processing Society Workshop (Cat. No.98TH8468).

Mika, S., Scholkopf, B., Smola, A.J., Muller, K.R., Scholz, M., Ratsch, G., 1999b. Kernel PCA and de-noising in feature spaces. Advances in Neural Information Processing Systems 11, 536-542.

Mildner, T., Norris, D.G., Schwarzbauer, C., Wiggins, C.J., 2001. A qualitative test of the balloon model for BOLD-based MR signal changes at 3T. Magn Reson Med 46, 891-899.

Minagawa-Kawai, Y., van der Lely, H., Ramus, F., Sato, Y., Mazuka, R., Dupoux, E., 2011. Optical brain imaging reveals general auditory and language-specific processing in early infant development. Cereb Cortex 21, 254-261.

Obrig, H., Israel, H., Kohl-Bareis, M., Uludag, K., Wenzel, R., Muller, B., Arnold, G., Villringer, A., 2002. Habituation of the visually evoked potential and its vascular response: implications for neurovascular coupling in the healthy adult. NeuroImage 17, 1-18.

Saitou, H., Yanagi, H., Hara, S., Tsuchiya, S., Tomura, S., 2000. Cerebral blood volume and oxygenation among poststroke hemiplegic patients: effects of 13 rehabilitation tasks measured by near-infrared spectroscopy. Arch Phys Med Rehabil 81, 1348-1356.

Sato, H., Aoki, R., Katura, T., Matsuda, R., Koizumi, H., 2011. Correlation of within-individual fluctuation of depressed mood with prefrontal cortex activity during verbal working memory task: optical topography study. J Biomed Opt 16, 126007.

Sato, H., Fuchino, Y., Kiguchi, M., Katura, T., Maki, A., Yoro, T., Koizumi, H., 2005. Intersubject variability of near-infrared spectroscopy signals during sensorimotor cortex activation. J Biomed Opt 10, 44001.

Sato, H., Tanaka, N., Uchida, M., Hirabayashi, Y., Kanai, M., Ashida, T., Konishi, I., Maki, A., 2006. Wavelet analysis for detecting body-movement artifacts in optical topography signals. NeuroImage 33, 580-587.

Sato, H., Yahata, N., Funane, T., Takizawa, R., Katura, T., Atsumori, H., Nishimura, Y., Kinoshita, A., Kiguchi, M., Koizumi, H., Fukuda, M., Kasai, K., 2013. A NIRS-fMRI investigation of

prefrontal cortex activity during a working memory task. NeuroImage 83C, 158-173.

Scholkmann, F., Gerber, U., Wolf, M., Wolf, U., 2013. End-tidal CO(2): An important parameter for a correct interpretation in functional brain studies using speech tasks. NeuroImage 66C, 71-79.

Sheth, S.A., Nemoto, M., Guiou, M., Walker, M., Pouratian, N., Toga, A.W., 2004. Linear and nonlinear relationships between neuronal activity, oxygen metabolism, and hemodynamic responses. Neuron 42, 347-355.

Sirotin, Y.B., Cardoso, M., Lima, B., Das, A., 2012. Spatial homogeneity and task-synchrony of the trial-related hemodynamic signal. NeuroImage 59, 2783-2797.

Sirotin, Y.B., Das, A., 2009. Anticipatory haemodynamic signals in sensory cortex not predicted by local neuronal activity. Nature 457, 475-479.

Sirotin, Y.B., Hillman, E.M., Bordier, C., Das, A., 2009. Spatiotemporal precision and hemodynamic mechanism of optical point spreads in alert primates. Proc Natl Acad Sci U S A 106, 18390-18395.

Soltysik, D.A., Peck, K.K., White, K.D., Crosson, B., Briggs, R.W., 2004. Comparison of hemodynamic response nonlinearity across primary cortical areas. NeuroImage 22, 1117-1127.

Steinbrink, J., Villringer, A., Kempf, F., Haux, D., Boden, S., Obrig, H., 2006. Illuminating the BOLD signal: combined fMRI-fNIRS studies. Magn Reson Imaging 24, 495-505.

Strangman, G., Boas, D.A., Sutton, J.P., 2002. Non-invasive neuroimaging using near-infrared light. Biol Psychiatry 52, 679-693.

Tachtsidis, I., Leung, T.S., Chopra, A., Koh, P.H., Reid, C.B., Elwell, C.E., 2009. False positives in functional nearinfrared topography. Oxygen Transport to Tissue XXX, 307-314.

Taga, G., Konishi, Y., Maki, A., Tachibana, T., Fujiwara, M., Koizumi, H., 2000. Spontaneous oscillation of oxy- and deoxy- hemoglobin changes with a phase difference throughout the occipital cortex of newborn infants observed using non-invasive optical topography. Neurosci

Lett 282, 101-104.

Takahashi, T., Takikawa, Y., Kawagoe, R., Shibuya, S., Iwano, T., Kitazawa, S., 2011. Influence of skin blood flow on near-infrared spectroscopy signals measured on the forehead during a verbal fluency task. NeuroImage 57, 991-1002.

Tanaka, H., Katura, T., Sato, H., 2013. Task-related component analysis for functional neuroimaging and application to near-infrared spectroscopy data. NeuroImage 64, 308-327.

Tang, L., Avison, M.J., Gore, J.C., 2009. Nonlinear blood oxygen level-dependent responses for transient activations and deactivations in V1 - insights into the hemodynamic response function with the balloon model. Magn Reson Imaging 27, 449-459.

Tong, Y., Hocke, L.M., Frederick, B., 2011. Isolating the sources of widespread physiological fluctuations in functional near-infrared spectroscopy signals. J Biomed Opt 16, 106005.

Toyoda, H., Kashikura, K., Okada, T., Nakashita, S., Honda, M., Yonekura, Y., Kawaguchi, H., Maki, A., Sadato, N., 2008. Source of nonlinearity of the BOLD response revealed by simultaneous fMRI and NIRS. NeuroImage 39, 997-1013.

Wolf, M., Wolf, U., Toronov, V., Michalos, A., Paunescu, L.A., Choi, J.H., Gratton, E., 2002. Different time evolution of oxyhemoglobin and deoxyhemoglobin concentration changes in the visual and motor cortices during functional stimulation: a near-infrared spectroscopy study. NeuroImage 16, 704-712.

Wyatt, J.S., Cope, M., Delpy, D.T., Richardson, C.E., Edwards, A.D., Wray, S., Reynolds, E.O., 1990. Quantitation of cerebral blood volume in human infants by near-infrared spectroscopy. J Appl Physiol (1985) 68, 1086-1091.

Wyatt, J.S., Cope, M., Delpy, D.T., Wray, S., Reynolds, E.O., 1986. Quantification of cerebral oxygenation and haemodynamics in sick newborn infants by near infrared spectrophotometry. Lancet 2, 1063-1066.

Wylie, G.R., Graber, H.L., Voelbel, G.T., Kohl, A.D., DeLuca, J., Pei, Y., Xu, Y., Barbour, R.L., 2009. Using co-variations in the Hb signal to detect visual activation: a near infrared spectroscopic imaging study. NeuroImage 47, 473-481.

Yamada, T., Umeyama, S., Matsuda, K., 2012. Separation of fNIRS signals into functional and systemic components based on differences in hemodynamic modalities. PLoS One 7, e50271.

Yamashita, Y., Maki, A., Koizumi, H., 2001. Wavelength dependence of the precision of noninvasive optical measurement of oxy-, deoxy-, and total-hemoglobin concentration. Med Phys 28, 1108-1114.

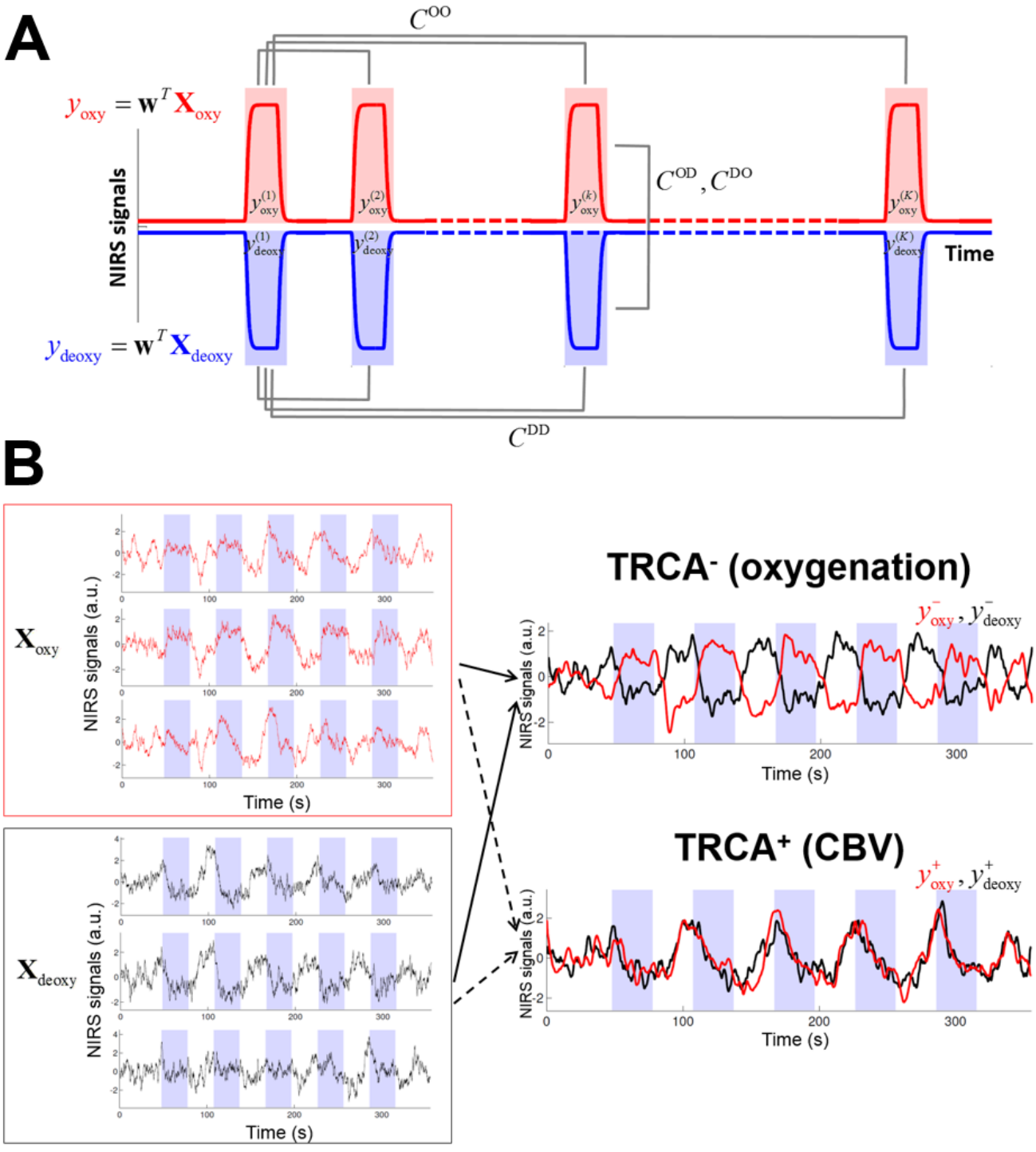

Figure 1.

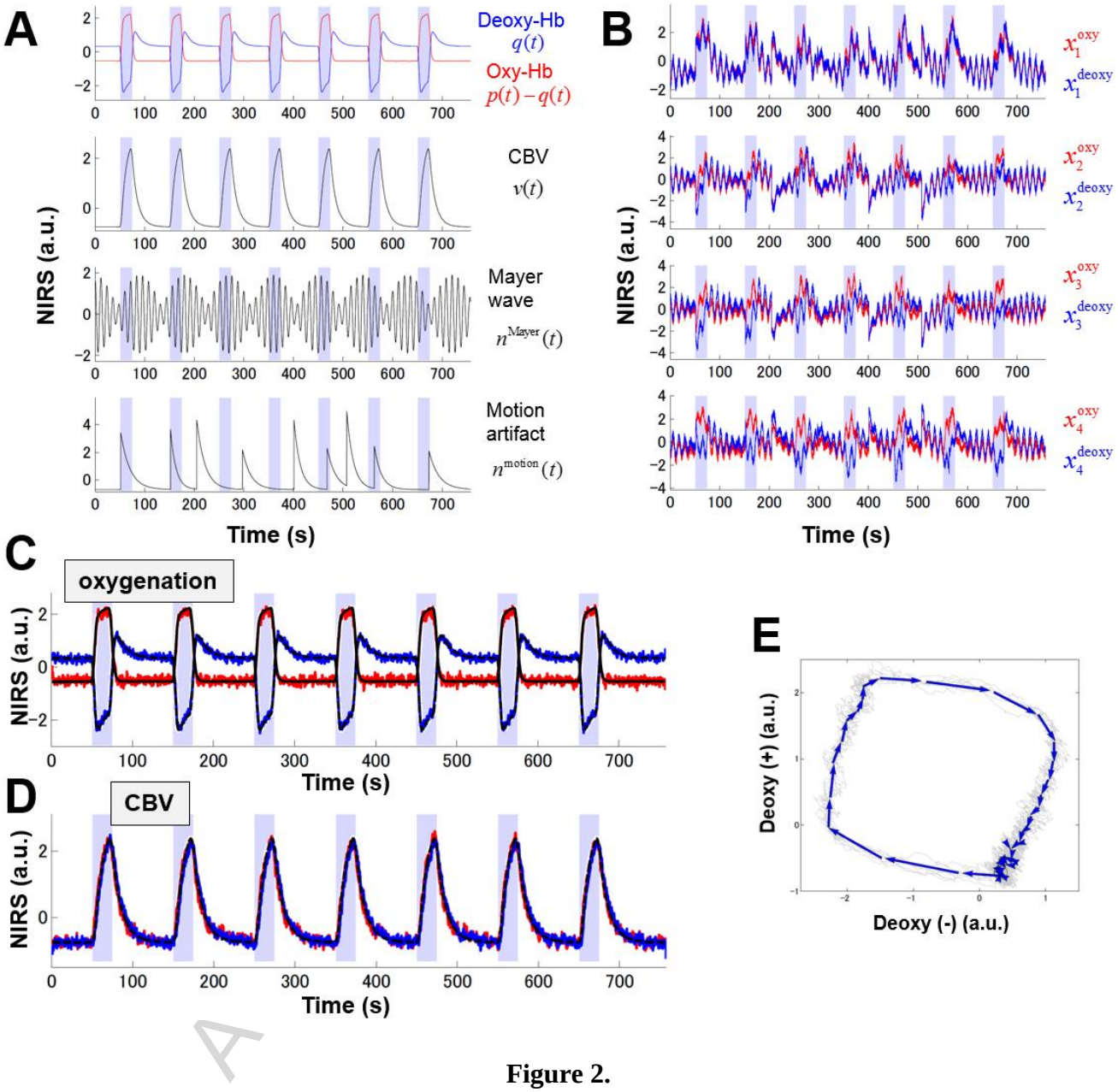

Figure 2.

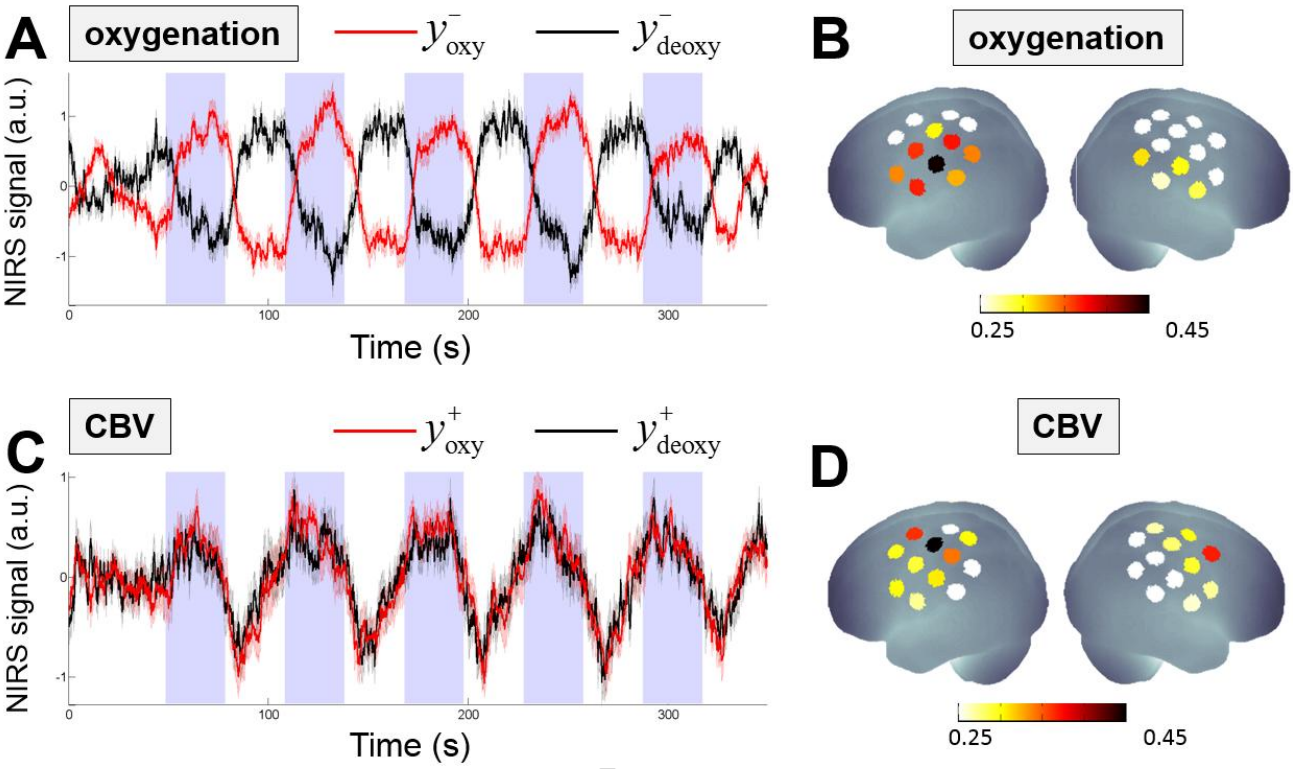

Figure 3.

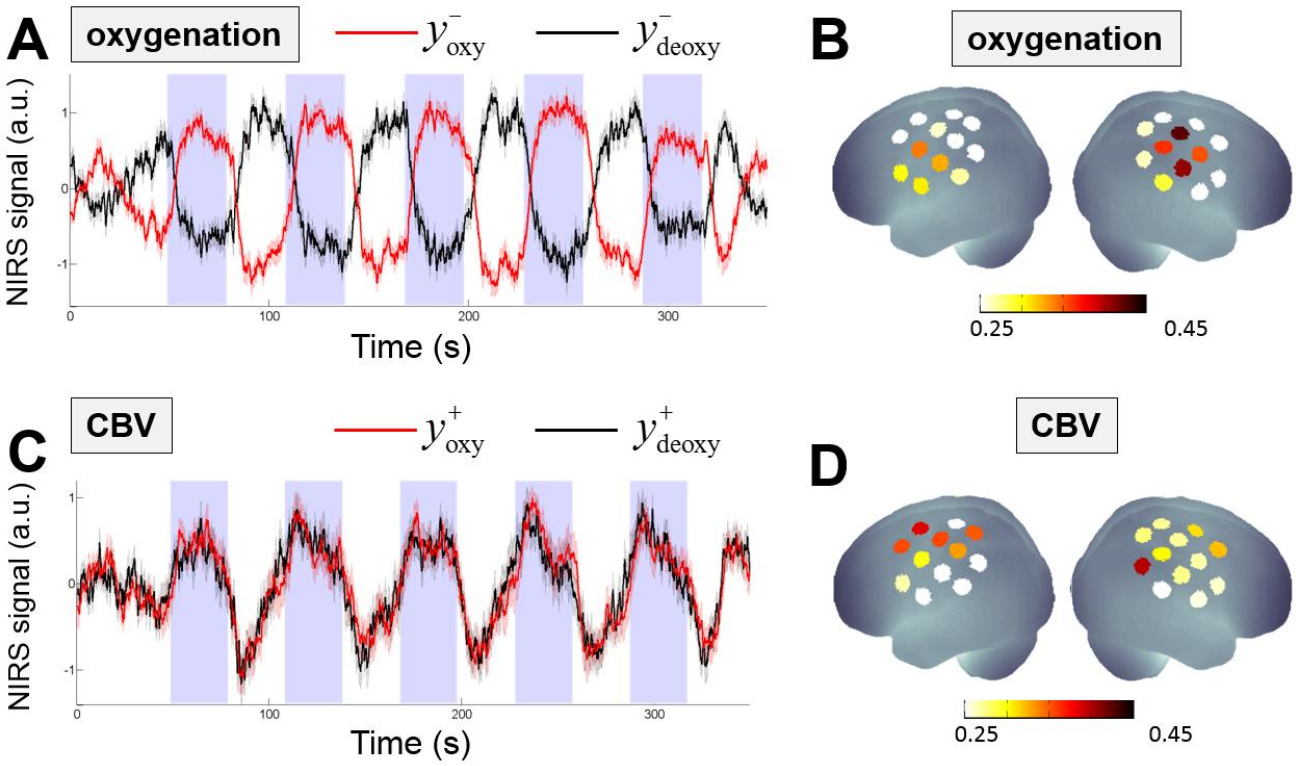

Figure 4

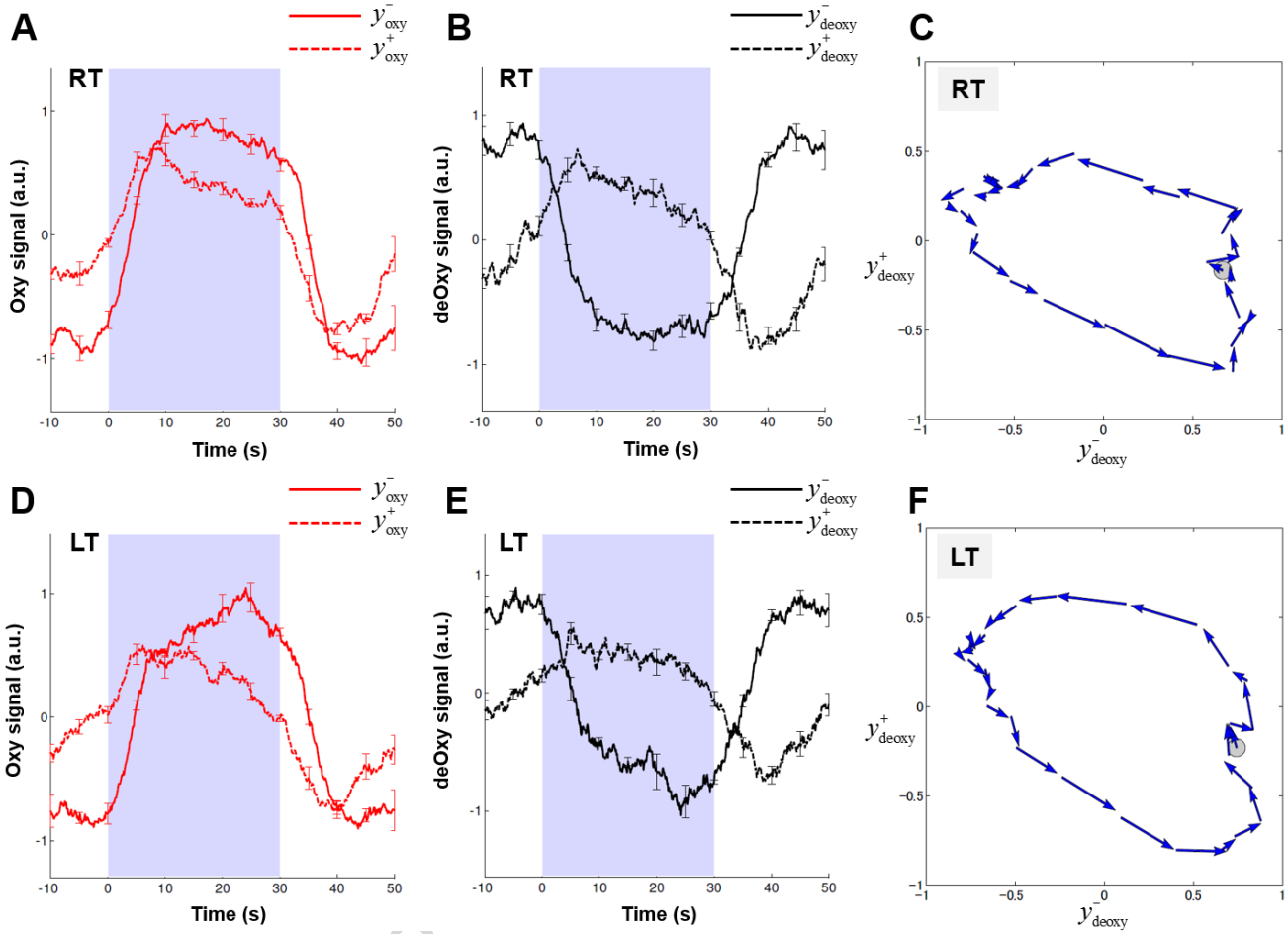

Figure 5

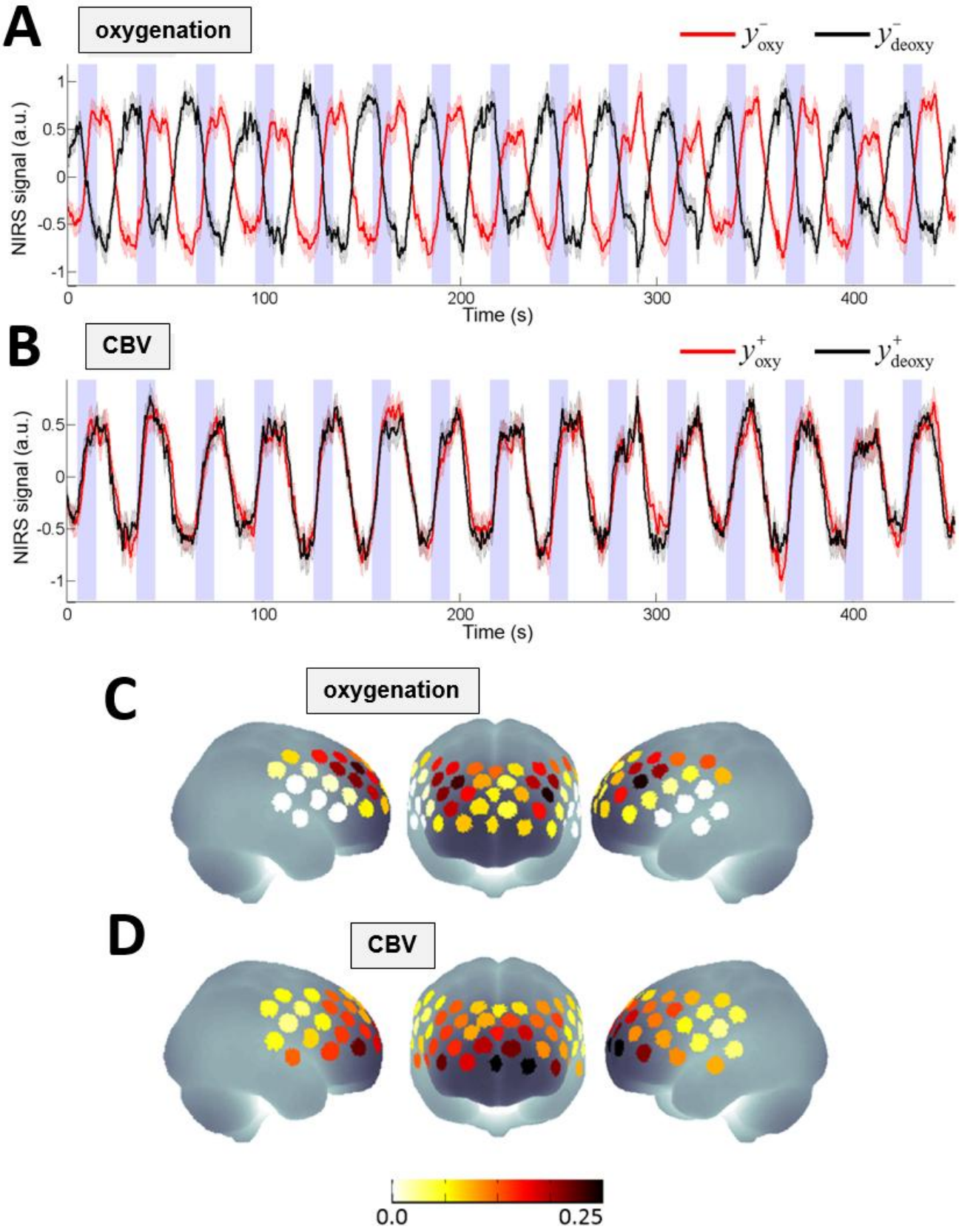
A
oxygenation
y^{-}_{oxy}
y^{-}_{deoxy}
NIRS signal (a.u.)
1
0.5
0
-0.5
-1
0
100
200
300
400
Time (s)
B
CBV
y^{+}_{oxy}
y^{+}_{deoxy}
NIRS signal (a.u.)
0.5
0
-0.5
-1
0
100
200
300
400
Time (s)
C
oxygenation
D
CBV
0.0
0.25

Figure 6

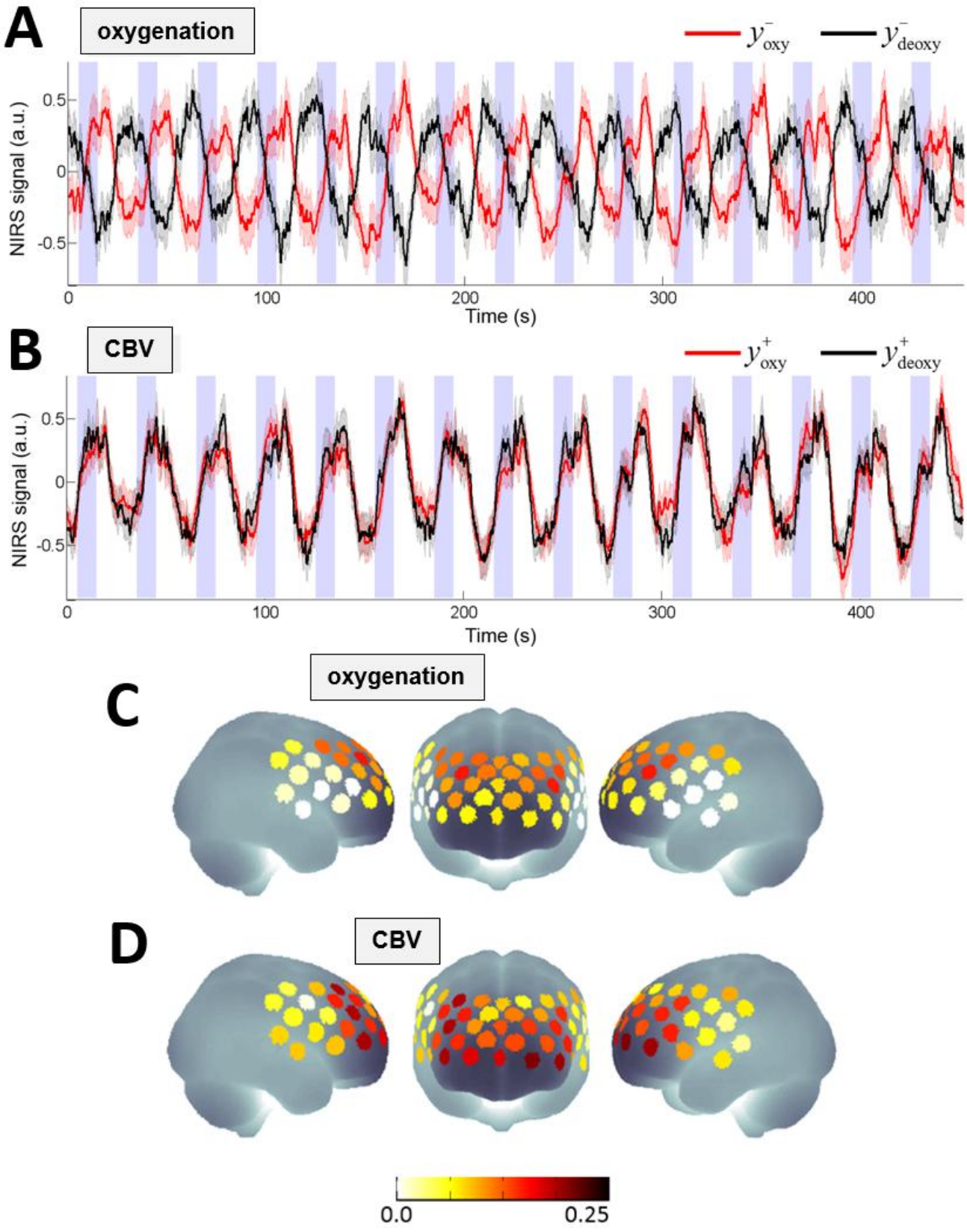
A
oxygenation
y^{-}_{oxy}
y^{-}_{deoxy}
NIRS signal (a.u.)
0.5
0
-0.5
0
100
200
300
400
Time (s)
B
CBV
y^{+}_{oxy}
y^{+}_{deoxy}
NIRS signal (a.u.)
0.5
0
-0.5
0
100
200
300
400
Time (s)
C
oxygenation
D
CBV
0.0
0.25

Figure 7

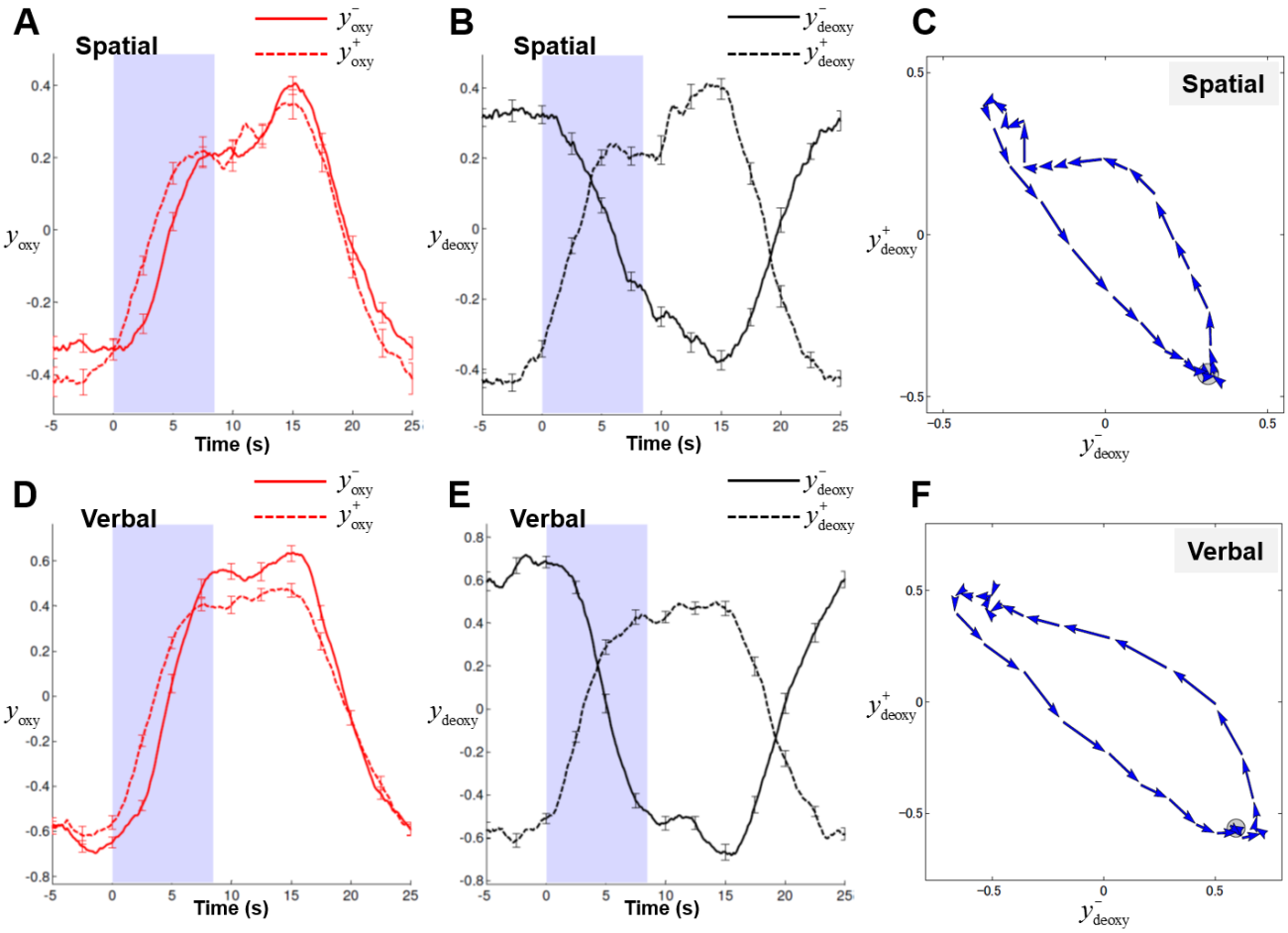

Figure 8